CHINESE OPTICS LETTERS

Vol. 21, No. 9 | September 2023

Experimental realization of strong coupling between a cold atomic ensemble and an optical fiber microcavity

Li Li (李 黎)[1,2], Yu-Hao Pan (潘宇豪)[1,2], Yi-Jia Liu (刘毅嘉)[1,2], Xiao-Long Zhou (周小龙)[1,2], Dong-Yu Huang (黄冬郁)[1,2], Ze-Min Shen (沈泽民)[1,2], Jian Wang (王 健)[1,2*], Chuan-Feng Li (李传锋)[1,2,3], and Guang-Can Guo (郭光灿)[1,2,3]

[1] CAS Key Laboratory of Quantum Information, University of Science and Technology of China, Hefei 230026, China

[2] CAS Center for Excellence in Quantum Information and Quantum Physics, University of Science and Technology of China, Hefei 230026, China

[3] Hefei National Laboratory, University of Science and Technology of China, Hefei 230088, China

*Corresponding author: jwang28@ustc.edu.cn

Received April 6, 2023 | Accepted June 2, 2023 | Posted Online August 18, 2023

The cavity quantum electrodynamics (QED) system is a promising platform for quantum optics and quantum information experiments. Its core is the strong coupling between atoms and optical cavity, which causes difficulty in the overlap between the atoms and the antinode of optical cavity mode. Here, we use a programmable movable optical dipole trap to load a cold atomic ensemble into an optical fiber microcavity and realize the strong coupling between the atoms and the optical cavity in which the coupling strength can be improved by polarization gradient cooling and adiabatic loading. By the measurement of vacuum Rabi splitting, the coupling strength can be as high as $g_N = 2\pi \times 400$ MHz, which means the effective atom number is $N_{\mathrm{eff}} = 16$ and the collective cooperativity is $C_N = 1466$. These results show that this experimental system can be used for cold atomic ensemble and cold molecule based cavity QED research.

Keywords: cavity quantum electrodynamics; optical fiber microcavity; strong coupling.
DOI: 10.3788/COL202321.092702

1. Introduction

The cavity quantum electrodynamics (QED) system is a platform for research of light–matter interaction that is important for quantum science and provides good test beds for quantum applications such as quantum communication[1], quantum simulation[2], and quantum computation[3–7]. The basis of the system is a single atom interacting with a single mode of an optical cavity, in which the atomic emission and optical cavity mode can be remarkably changed to coherently manipulate and detect the atomic state, and do the same to other matters such as quantum dots, trapped ions, and cold molecules[8–11]. The interaction between the atom and the optical cavity mode can support quantum applications, such as quantum-logic gate and quantum network node, and increase the scatter area of photons and atoms, which can be used as single photon sources[12–18]. The atomic ensemble in the optical cavity can attain stronger interaction compared with a single atom due to the collective action, and has been increasingly involved in ultracold quantum gases and quantum precision measurement and sensing[19–27].

The strong coupling regime is a core of the cavity QED system, which has been realized with matters such as cold atoms, trapped ions, quantum dots, and organic molecules[28–34]. The coupling strength g represents the interaction between the atom and the optical cavity mode, and the dissipative rates are cavity-field decay rate κ and atomic decay rate γ[35–39]. Cooperativity, denoted by C, is commonly used to characterize this regime when it is bigger than unity and when g is bigger than κ and γ,

$$C = \frac{g^2}{2\kappa\gamma}, \tag{1}$$

$$g = d\sqrt{\frac{\pi\omega_c}{h\varepsilon_0 V}}, \tag{2}$$

where d is the electric dipole moment, ε_0 is the vacuum permittivity, h is the Planck's constant, ω_c is the optical cavity mode resonant frequency, and V represents the optical cavity mode volume. To reach the strong coupling regime, the coupling strength must be large enough so the optical cavity mode is generally designed to be sufficiently tiny, as shown in Eq. (2). A fiber-based microcavity integrated on optical fibers allows for small open quantum devices with favorable scaling properties, including structure stability and tiny volume[40–46]. The small size at the micrometer scale followed by applicable mode volume can support the strong coupling with atoms and be conveniently integrated into the fiber-based quantum system. Cold atoms are

commonly prepared by a magneto-optical trap (MOT) and normally cannot be directly formed in such a microcavity instead by transporting atoms from the MOT to the optical cavity. The transport scheme mostly contains two ways of moving the magnetic trap, which uses a movable anti-Helmholz coil pair or a magnetic quadrupole trap[47,48], and moves through an optical dipole trap, which is achieved by an adjustable lens or an optical conveyor belt using an optical lattice[49–52]. During the transport process, it is significant to prevent atoms from heating and attain a loading efficiency that gets enough atoms into the optical cavity mode for strong coupling. Polarization gradient cooling (PGC) and adiabatic loading are used to attain these requirements, which can decrease atomic temperature and load more atoms into the optical cavity mode.

Here, we use a programmable movable optical dipole trap (ODT) at 1064 nm to transport the cold atomic ensemble from the MOT into the optical fiber microcavity mode, and the accuracy attains the requirements for maximal strong coupling. Then the spectrum of the coupled atom–cavity is scanned out, which shows the strong coupling is realized. The PGC and adiabatic loading are performed to improve the coupling strength, which increases the g_N to $2\pi \times 400$ MHz followed by the effective atom number N_{eff} of 16 and the collective cooperativity C_N of 1466. The results show good strong coupling of the system, which can be used to enhance the molecular formation and nondestructively measure it by detecting the emitted photons collected by the optical fiber microcavity during the formation process[53,54]. Owing to the small mode volume of the optical fiber microcavity, the formed molecules can be used to realize strong coupling and other relevant cold molecule cavity QED experiments[55,56].

2. Experiment and Results

2.1. Experimental setup

The cold ^{85}Rb atom is prepared by a MOT in the D2 line ($\gamma = 2\pi \times 3.03$ MHz). The trapping laser is 12 MHz red-detuned with the cycling transition $|F = 3\rangle \rightarrow |F' = 4\rangle$, and the repumping transition is resonant with $|F = 2\rangle \rightarrow |F' = 3\rangle$. The radius of the trapping and repumping laser beam is about 2 mm, which forms the MOT with a diameter of about 800 μm. The cavity length of the optical fiber microcavity is about 113 μm, and the decay rate $\kappa = 2\pi \times 18$ MHz [half the full width at half-maximum (FWHM)][41]. The optical cavity mode that resonates with atom transition ω_a is locked to the 850 nm cavity longitudinal mode frequency. which forms the 850 nm optical lattice to trap atoms. The resonant transition ω_a is resonant with $|F = 3\rangle \rightarrow |F' = 4\rangle$ and is employed to probe the coupled system. The coupling strength g_0 is expected to be $2\pi \times 97.5$ MHz, which is the best coupled case when a single atom is placed at the center of the optical cavity mode. The MOT is formed below the optical fiber microcavity with 5 mm for its big scale so the atomic ensemble is transported from the MOT to the optical fiber microcavity.

The transport scheme is realized by a programmable movable optical dipole trap with a 10 W fiber laser at 1064 nm and an acousto-optic deflector (AOD), as shown in Fig. 1(a). The diameter of the fiber laser beam is expanded from 1 to 5 mm by a lens group before being diffracted by the AOD with an active aperture of 7 mm. The first diffracted laser beam is used and focused through a 125 mm achromatic lens to a diameter of 30 μm onto the MOT, which can cover the optical cavity mode with a waist radius of 4.9 μm and avoid shining on the optical fiber microcavity. When focused into the optical cavity, the 1064 nm laser power at MOT goes down linearly from 4 W to 500 mW, which can reduce the thermal effect of the optical fiber microcavity caused by the high-power laser[57,58]. To precisely transport atoms, a programmable arbitrary waveform generator (AWG) is used to generate the microwave amplified by a microwave amplifier to drive the AOD and keep the diffraction efficiency above 75% throughout the transport process. The angle of the first diffracted laser beam is changed to transport the atoms

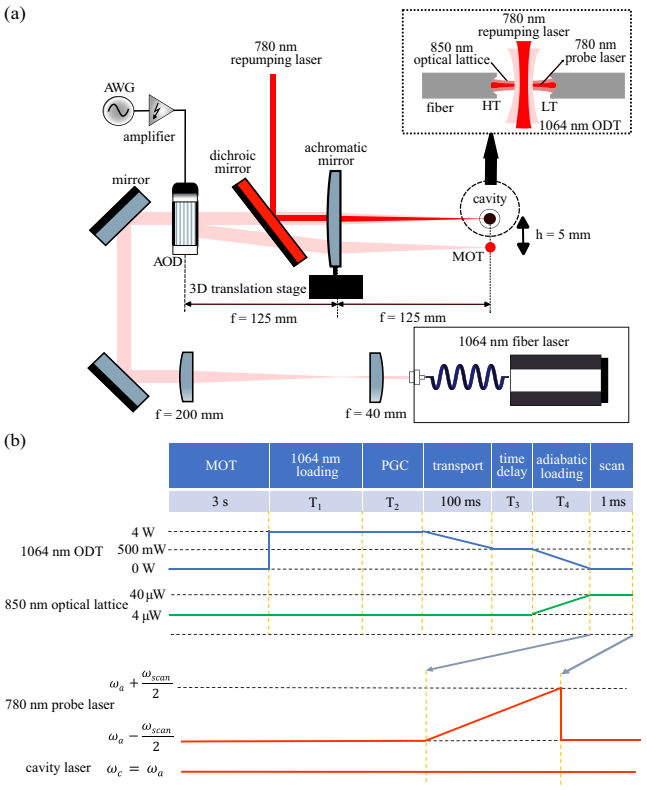

Fig. 1. (a) Schematic diagram of the transport setup from MOT to the optical cavity mode. The 1064 nm ODT and 780 nm repumping laser beams are combined with a dichroic mirror and focused through an achromatic lens. The atoms are trapped in the 850 nm optical lattice, and the 780 nm probe laser is along the optical cavity axis, shown in the upper right. The 850 nm and 780 nm lasers are coupled into the optical cavity mode from the HT cavity mirror. HT, high-transmission cavity mirror; LT, low-transmission cavity mirror; (b) Experimental time sequence; T_1, T_2, T_3, and T_4 are different values in followed transport strategies. The ω_c is the optical cavity resonant frequency, and the ω_{scan} is the scanning width of the 780 nm probe frequency.

by altering the frequency of the microwave. The cosine profile is adopted for the transport velocity and the microwave signal S is described by

$$S = \sin\ \varphi, \tag{3}$$

$$\frac{\mathrm{d}\varphi}{dt} = 2\pi[A + B\ \cos(\pi\omega_0 t)], \tag{4}$$

$$A = \omega_1 + \frac{\omega_2 - \omega_1}{2}, \quad B = \frac{\omega_2 - \omega_1}{2}, \quad \omega_0 = \frac{1}{\mathrm{T}}, \tag{5}$$

where ω_1 and ω_2 are the microwave frequencies of diffracting the laser beam at the positions of the optical cavity and the MOT, respectively, and T is the transport time duration with a value of 100 ms, as shown in Fig. 1(b). With the active acceleration-
deceleration strategy, the transport scheme provides adequate atoms and reduces motion heating, as shown in Fig. 2.

To ensure the best overlap between the atomic ensemble and the optical cavity mode, the first diffracted laser waist is required to be placed at the center of the mode where the atom cavity is mostly coupled. The mismatch between the waist and the center is minimized by adjusting the microwave frequency of the AWG and the position of the 125 mm lens, which is placed at a 3D translation stage, as shown in Fig. 1(a). The geometrical center of the MOT is placed at the center of 1064 nm ODT where the atomic loading from MOT to the ODT is optimal by adjusting the 780 nm laser beam path and the position of magnetic field

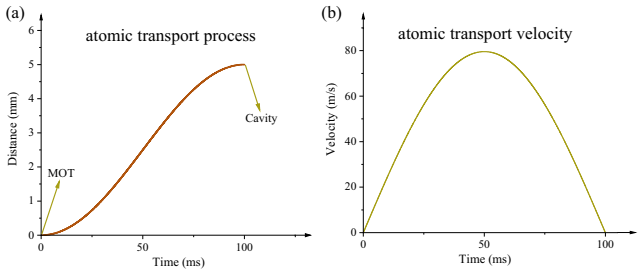

Fig. 2. (a) Transport process of the atoms from MOT to the optical cavity. (b) The atoms' velocity profile is the active acceleration-deceleration strategy.

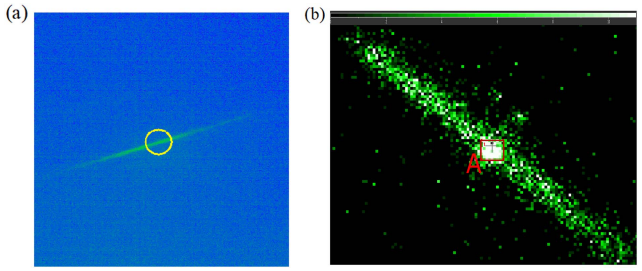

Fig. 3. (a) Image of the 1064 nm ODT at MOT. The yellow ring is the location of the MOT. (b) Image of the 1064 nm ODT at the position of optical cavity; the A rectangular box represents atomic fluorescence in the optical cavity.

coil. To pinpoint the atoms in the optical cavity mode, we use two cameras (CMOS-DC1240x and EMCCD-iXon 888) to separately image the 1064 nm ODT at the MOT and the optical cavity, as shown in Fig. 3. In Fig. 3(b), 780 nm MOT trapping laser is used to excite the atoms and the atomic fluorescence is collected for imaging. The atomic fluorescence in the optical cavity is stronger than other parts of the 1064 nm ODT, which can determine the height position of 1064 nm ODT by making the brightest fluorescence with the 125 mm lens and the AWG.

2.2. Results

To probe the strongly coupled system, the vacuum Rabi splitting (VRS) with the value corresponding to $2g$ is measured, which characterizes the coupling strength of the atom–cavity system[59–61]. For the atomic ensemble and the optical cavity mode, the collective coupling constant is $g_N = \sqrt{N_{\mathrm{eff}}} \cdot g_0$, in which N_{eff}, called the effective atom number, shows the equivalent number of the atoms in the best coupled case and the collective cooperativity is $C_N = N_{\mathrm{eff}} \cdot C_0$. Due to the good coupling strength of the system requiring a wide range of the frequency sweeping, the energy spectrum is obtained by scanning the frequency of a 780 nm distributed feedback (DFB) laser controlled by diode current. The spectrum shows the VRS when the atomic ensemble is accurately loaded into the optical cavity mode, and provides the collective coupling constant g_N followed by the collective cooperativity C_N and the effective atom number N_{eff}. The experimental time sequence is described by Fig. 1(b), and the atomic ensemble is directly transported to the optical cavity with $\mathrm{T}_1 = 500$ ms, $\mathrm{T}_2 = 0$ ms, $\mathrm{T}_3 = 15$ ms, and $\mathrm{T}_4 = 0$ ms. The 1064 nm ODT power in the optical cavity is 500 mW, and the 850 nm power before the fiber coupling input is 40 μW. The probe photon counts are collected by a single-photon counter, which is set suitably for the optimal signal-to-noise ratio. In Fig. 4, the spectrum of the system is scanned out with a width of $\omega_{\mathrm{scan}} = 750$ MHz. The reflection spectrum shows no significant splitting but rather a photon blockade. The transmission spectrum exhibits a little frequency shift, and the photon counts are far below the reflected counts because it is being collected from the low-transmission (LT) cavity mirror, as shown in Fig. 1(a). The photon blockade shows inefficient transport with a small effective atom number followed by a little g_N, and this can be illustrated by the transport process and the direct loading heat and loss of the atoms.

3. Coupling Strength Optimization

Before transporting the atoms, polarization gradient cooling is performed to lower the atomic temperature, which improves the atom–cavity coupling strength as follows[62,63]. To load more atoms into the 850 nm optical lattice, the adiabatic loading scheme is chosen, as the 850 nm laser power ramps up while the 1064 nm power goes down. Different transport strategies are compared, and the corresponding VRS is scanned out as follows.

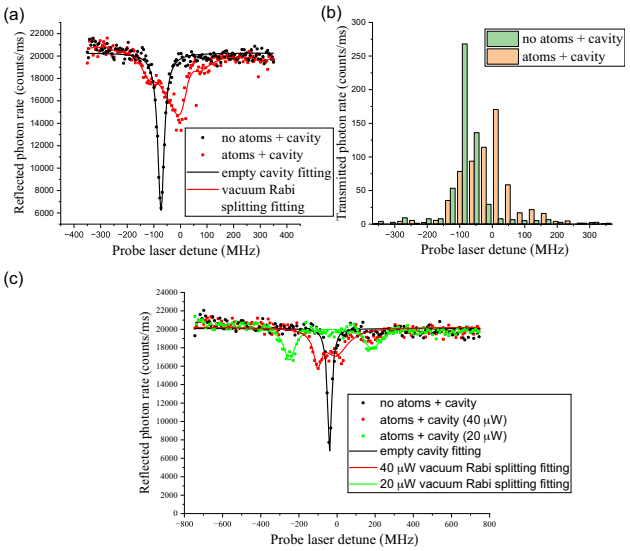

Fig. 4. Measurement of vacuum Rabi splitting. (a) Reflection spectrum of the atom–cavity system. Scatter is the experimental data. The black line is the Lorentz fitting of the cavity reflection spectrum and the red line is the vacuum Rabi splitting fitting. (b) Transmission spectrum of the atom–cavity system; the column is the experimental data. (c) The optimized reflection spectrum of the optimization with PGC in different 850 nm laser powers.

3.1. PGC

Before transporting atoms, the PGC is performed with time durations $T_1 = 490$ ms and $T_2 = 10$ ms, while the 850 nm power is still 40 μW and the scanning width ω_{scan} is 1600 MHz. As shown in Fig. 4(c), there is a little VRS of $2\pi \times 90$ MHz that represents the effective atom number $N_{\text{eff}} = 0.2$ and the collective cooperativity $C_N = 18$. This shows the strong coupling and illustrates that PGC improves atomic transport efficiency.

To investigate the influence of trap depth of the 850 nm optical lattice, the power of the 850 nm laser is reduced to 20 μW. The VRS with $2\pi \times 421$ MHz is attained, which represents the effective atom number $N_{\text{eff}} = 4$ and the collective cooperativity $C_N = 404$ in Fig. 4(c). The stronger coupling shows a shallower depth of the 850 nm optical lattice helps load more atoms into the optical cavity mode with less collision loss, but it is not conducive to certain experiments that require atomic collision and long trap time.

3.2. Adiabatic loading

To transport more atoms into the high-depth trap, adiabatic loading is proposed to ramp the 1064 nm ODT power down while ramping the 850 nm power up. The atomic ensemble is directly transported without PGC for comparison, and in the optical cavity, the 1064 nm power linearly descends; meanwhile, the 850 nm power linearly rises from 4 to 40 μW with time durations $T_3 = 5$ ms and $T_4 = 10$ ms. In Table 1, the VRS is $2\pi \times 640$ MHz, where the effective atom number $N_{\text{eff}} = 10$ and the collective cooperativity $C_N = 938$, which means there is a good strong coupling.

Table 1. Results of the Strong Coupling Correspond to Different Transport Strategies.

Transport Strategy	C_N	g_N (MHz)	N_{eff}
PGC + no adiabatic loading	18	$2\pi \times 45$	0.2
no PGC + adiabatic loading	938	$2\pi \times 320$	10
PGC + adiabatic loading	1466	$2\pi \times 400$	16

The result shows the adiabatic loading can effectively load the atoms into the optical cavity mode. And it means that atoms can be loaded into the high-depth trap while holding a well N_{eff}. The scheme is useful for atomic storage and collision experiments, such as cavity-controlled molecular formation.

3.3. PGC and adiabatic loading

The PGC and adiabatic loading are combined with time durations $T_1 = 490$ ms, $T_2 = 10$ ms, $T_3 = 5$ ms, and $T_4 = 10$ ms. The VRS of $2\pi \times 800$ MHz is achieved, corresponding to the effective atom number $N_{\text{eff}} = 16$ and the collective cooperativity $C_N = 1466$, which represents a fairly good strong coupling. As shown in Fig. 5, the splitting peak of the spectrum is smaller than the optical cavity peak due to the larger detuning, and the transmission spectrum also shows a visible splitting due to the good VRS. The result can be used in relevant experiments such as the optical switch and cavity-controlled molecular formation[35,53,54].

Atoms will fall into different internal states due to incoherent processes such as atomic collision, so the MOT repumping laser is applied to optical pump atoms at the optical cavity into the $|F = 3\rangle$ level along the radial direction when loading the atoms into the optical cavity mode, as shown in Fig. 1(a), upper right. When the radial 780 nm repumping laser is tuned to the 780 nm cooling laser, which will pump the atoms into the $|F = 2\rangle$ level, there is a frequency shift instead of VRS that is described by

$$\Delta_{\text{shift}} = \frac{g_N'^2}{\Delta_c}, \tag{6}$$

$$\Delta_c = \omega_c - \omega_a', \tag{7}$$

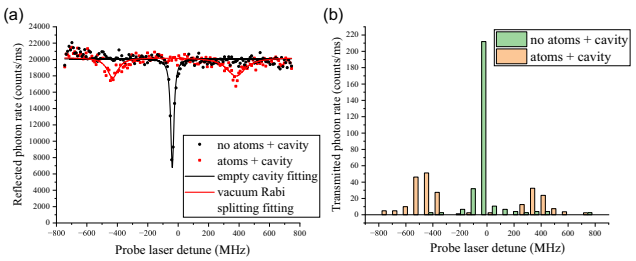

Fig. 5. (a) Optimized reflection spectrum with PGC and adiabatic loading. (b) Optimized transmission spectrum in which the VRS is visible.

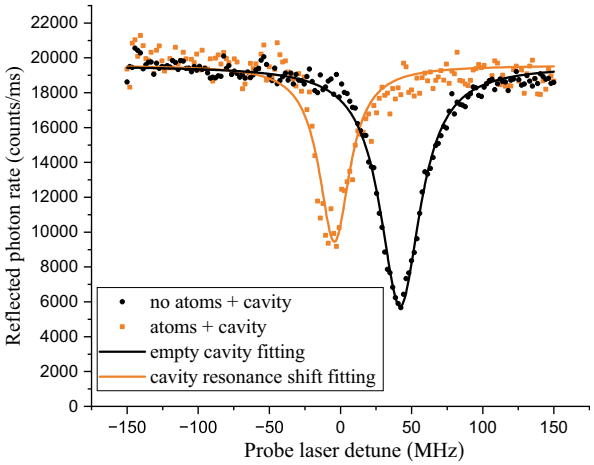

Fig. 6. Frequency shift of atoms in the $|F=2\rangle$ level, which is pumped by the 780 nm cooling laser.

where ω_c is the optical cavity resonant frequency, and ω_a' is the atomic resonant frequency. As shown in Fig. 6, there is a frequency shift of $2\pi \times 47$ MHz corresponding to the effective atom number $N_{\text{eff}}' = 14$, which is nearly equal to the $N_{\text{eff}} = 16$. The obviously different phenomenon shows that the strong coupling system can be used to detect the atomic internal state.

4. Conclusion

In this paper, we load atoms into an optical fiber microcavity by a programmable movable optical dipole trap and attain the atom–cavity strong coupling regime, benefiting from the good coupling constant g_0 and the effective atomic transport. The VRS is optimized to $2\pi \times 800$ MHz and represents that the effective atom number N_{eff} is 16 and the collective cooperativity C_N is 1466 with PGC and adiabatic loading, which means a good strong coupling. The appealing results show that the atom–cavity system can be used for cavity-enhancing molecular formation and support cold molecule cavity QED experiments, such as the strong coupling between cold molecules and optical cavities[28–32,53–56].

Acknowledgement

This work was supported by the Innovation Program for Quantum Science and Technology (No. 2021ZD0301200), the National Natural Science Foundation of China (Nos. 11804330 and 11821404), and the Fundamental Research Funds for the Central Universities (WK2470000038).

References

1. N. Gisin and R. Thew, "Quantum communication," Nat. Photonics **1**, 165 (2007).
2. I. M. Georgescu, S. Ashhab, and F. Nori, "Quantum simulation," Rev. Mod. Phys. **86**, 153 (2014).
3. H. Walther, B. T. H. Varcoe, B.-G. Englert, and T. Becker, "Cavity quantum electrodynamics," Rep. Prog. Phys. **69**, 1325 (2006).
4. H. J. Kimble, "The quantum internet," Nature **453**, 1023 (2008).
5. A. Reiserer and G. Rempe, "Cavity-based quantum networks with single atoms and optical photons," Rev. Mod. Phys. **87**, 1379 (2015).
6. N. Meher and S. Sivakumar, "A review on quantum information processing in cavities," Eur. Phys. J. Plus **137**, 985 (2022).
7. T. D. Ladd, F. Jelezko, R. Laflamme, Y. Nakamura, C. Monroe, and J. L. O'Brien, "Quantum computers," Nature **464**, 45 (2010).
8. J. A. Muniz, D. Barberena, R. J. Lewis-Swan, D. J. Young, J. R. K. Cline, A. M. Rey, and J. K. Thompson, "Exploring dynamical phase transitions with cold atoms in an optical cavity," Nature **580**, 602 (2020).
9. D. Najer, I. Söllner, P. Sekatski, V. Dolique, M. C. Löbl, D. Riedel, R. Schott, S. Starosielec, S. R. Valentin, A. D. Wieck, N. Sangouard, A. Ludwig, and R. J. Warburton, "A gated quantum dot strongly coupled to an optical microcavity," Nature **575**, 622 (2019).
10. H. Takahashi, E. Kassa, C. Christoforou, and M. Keller, "Cavity-induced backaction in Purcell-enhanced photon emission of a single ion in an ultraviolet fiber cavity," Phys. Rev. A. **95**, 033812 (2017).
11. B. P. Lanyon, J. D. Whitfield, G. Gillett, M. E. Goggin, M. P. Almeida, I. Kassal, J. D. Biamonte, M. Mohseni, B. J. Powell, M. Barbieri, A. Aspuru-Guzik, and A. G. White, "Towards quantum chemistry on a quantum computer," Nat. Chem. **2**, 106 (2010).
12. B. Hacker, S. Welte, G. Rempe, and S. Ritter, "A photon–photon quantum gate based on a single atom in an optical resonator," Nature **536**, 193 (2016).
13. S. Daiss, S. Langenfeld, S. Welte, E. Distante, P. Thomas, L. Hartung, O. Morin, and G. Rempe, "A quantum-logic gate between distant quantum-network modules," Science **371**, 614 (2021).
14. M. Brekenfeld, D. Niemietz, J. D. Christesen, and G. Rempe, "A quantum network node with crossed optical fibre cavities," Nature **16**, 647 (2020).
15. S. Ritter, C. Nölleke, C. Hahn, A. Reiserer, A. Neuzner, M. Uphoff, M. Mücke, E. Figueroa, J. Bochmann, and G. Rempe, "An elementary quantum network of single atoms in optical cavities," Nature **484**, 195 (2012).
16. M. Gessner, A. Smerzi, and L. Pezzè, "Multiparameter squeezing for optimal quantum enhancements in sensor networks," Nat. Commun. **11**, 3817 (2020).
17. C. Hamsen, K. N. Tolazzi, T. Wilk, and G. Rempe, "Two-photon blockade in an atom-driven cavity QED system," Phys. Rev. Lett. **118**, 133604 (2017).
18. A. Kuhn and D. Ljunggren, "Cavity-based single-photon sources," Contemp. Phys. **51**, 289 (2010).
19. R. Rosa-Medina, F. Ferri, F. Finger, N. Dogra, K. Kroeger, R. Lin, R. Chitra, T. Donner, and T. Esslinger, "Observing dynamical currents in a non-Hermitian momentum lattice," Phys. Rev. Lett. **128**, 143602 (2022).
20. F. Ferri, R. Rosa-Medina, F. Finger, N. Dogra, M. Soriente, O. Zilberberg, T. Donner, and T. Esslinger, "Emerging dissipative phases in a superradiant quantum gas with tunable decay," Phys. Rev. X **11**, 041046 (2021).
21. M. Landini, N. Dogra, K. Kroeger, L. Hruby, T. Donner, and T. Esslinger, "Formation of a spin texture in a quantum gas coupled to a cavity," Phys. Rev. Lett. **120**, 223602 (2018).
22. H. Ritsch, P. Domokos, F. Brennecke, and T. Esslinger, "Cold atoms in cavity-generated dynamical optical potentials," Rev. Mod. Phys. **85**, 553 (2013).
23. Z. Li, B. Braverman, S. Colombo, C. Shu, A. Kawasaki, A. F. Adiyatullin, E. Pedrozo-Peñafiel, E. Mendez, and V. Vuletić, "Collective spin-light and light-mediated spin-spin interactions in an optical cavity," PRX Quantum **3**, 020308 (2022).
24. F. Mivehvar, F. Piazza, T. Donner, and H. Ritsch, "Cavity QED with quantum gases: new paradigms in many-body physics," Adv. Phys. **70**, 1 (2021).
25. I. B. Mekhov and H. Ritsch, "Quantum optics with ultracold quantum gases: towards the full quantum regime of the light–matter interaction," J. Phys. B At. Mol. Opt. Phys. **45**, 102001 (2012).
26. M.-J. Hwang and M. B. Plenio, "Quantum phase transition in the finite Jaynes-Cummings lattice systems," Phys. Rev. Lett. **117**, 123602 (2016).
27. M. Hosseini, Y. Duan, K. M. Beck, Y.-T. Chen, and V. Vuletić, "Cavity cooling of many atoms," Phys. Rev. Lett. **118**, 183601 (2017).
28. Y. Colombe, T. Steinmetz, G. Dubois, F. Linke, D. Hunger, and J. Reichel, "Strong atom–field coupling for Bose–Einstein condensates in an optical cavity on a chip," Nature **450**, 272 (2007).

29. M. Koch, C. Sames, M. Balbach, H. Chibani, A. Kubanek, K. Murr, T. Wilk, and G. Rempe, "Three-photon correlations in a strongly driven atom-cavity system," Phys. Rev. Lett. **107**, 023601 (2011).
30. H. M. Meyer, R. Stockill, M. Steiner, C. Le Gall, C. Matthiesen, E. Clarke, A. Ludwig, J. Reichel, M. Atatüre, and M. Köhl, "Direct photonic coupling of a semiconductor quantum dot and a trapped ion," Phys. Rev. Lett. **114**, 123001 (2015).
31. H. Takahashi, E. Kassa, C. Christoforou, and M. Keller, "Strong coupling of a single ion to an optical cavity," Phys. Rev. Lett. **124**, 013602 (2020).
32. J. Miguel-Sánchez, A. Reinhard, E. Togan, T. Volz, A. Imamoglu, B. Besga, J. Reichel, and J. Estève, "Cavity quantum electrodynamics with charge-controlled quantum dots coupled to a fiber Fabry–Perot cavity," New J. Phys. **15**, 045002 (2013).
33. D. Wang, H. Kelkar, D. Martin-Cano, T. Utikal, S. Götzinger, and V. Sandoghdar, "Coherent coupling of a single molecule to a scanning Fabry-Perot microcavity," Phys. Rev. X **7**, 021014 (2017).
34. A. Pscherer, M. Meierhofer, D. Wang, H. Kelkar, D. Martín-Cano, T. Utikal, S. Götzinger, and V. Sandoghdar, "Single-molecule vacuum rabi splitting: four-wave mixing and optical switching at the single-photon level," Phys. Rev. Lett **127**, 133603 (2021).
35. P. Yang, X. Xia, H. He, S. Li, X. Han, P. Zhang, G. Li, P. Zhang, J. Xu, Y. Yang, and T. Zhang, "Realization of nonlinear optical nonreciprocity on a few-photon level based on atoms strongly coupled to an asymmetric cavity," Phys. Rev. Lett. **123**, 233604 (2019).
36. J. D. Thompson, T. G. Tiecke, N. P. de Leon, J. Feist, A. V. Akimov, M. Gullans, A. S. Zibrov, V. Vuletić, and M. D. Lukin, "Coupling a single trapped atom to a nanoscale optical cavity," Science **340**, 1202 (2013).
37. A. Kawasaki, B. Braverman, E. Pedrozo-Peñafiel, C. Shu, S. Colombo, Z. Li, ö. özel, W. Chen, L. Salvi, A. Heinz, D. Levonian, D. Akamatsu, Y. Xiao, and V. Vuletić, "Geometrically asymmetric optical cavity for strong atom-photon coupling," Phys. Rev. A **99**, 013437 (2019).
38. J. A. Sauer, K. M. Fortier, M. S. Chang, C. D. Hamley, and M. S. Chapman, "Cavity QED with optically transported atoms," Phys. Rev. A. **69**, 051804 (2004).
39. J. M. Raimond, M. Brune, and S. Haroche, "Manipulating quantum entanglement with atoms and photons in a cavity," Rev. Mod. Phys. **73**, 565 (2001).
40. D. Hunger, T. Steinmetz, Y. Colombe, C. Deutsch, T. W. Hänsch, and J. Reichel, "A fiber Fabry–Perot cavity with high finesse," New J. Phys. **12**, 065038 (2010).
41. Y. Pan, L. Li, X. Zhou, D. Huang, Z. Shen, J. Wang, C. Li, and G. Guo, "Fabrication, testing, and assembly of high-finesse optical fiber microcavity for molecule cavity QED experiment," Chin. Opt. Lett. **20**, 122702 (2022).
42. M. Ruf, M. J. Weaver, S. B. van Dam, and R. Hanson, "Resonant excitation and purcell enhancement of coherent nitrogen-vacancy centers coupled to a Fabry-Perot microcavity," Phys. Rev. Appl. **15**, 024049 (2021).
43. M. H. Bitarafan and R. G. DeCorby, "On-chip high-finesse Fabry-Perot microcavities for optical sensing and quantum information," Sensors **17**, 1748 (2017).
44. G. Kurizki, P. Bertet, Y. Kubo, K. Mølmer, D. Petrosyan, P. Rabl, and J. Schmiedmayer, "Quantum technologies with hybrid systems," Proc. Natl. Acad. Sci. U.S.A. **112**, 3866 (2015).
45. Y. Duan, M. Hosseini, K. M. Beck, and V. Vuletić, "Heralded interaction control between quantum systems," Phys. Rev. Lett. **124**, 223602 (2020).
46. J.-M. Cui, K. Zhou, M.-S. Zhao, M.-Z. Ai, C.-K. Hu, Q. Li, B.-H. Liu, J.-L. Peng, Y.-F. Huang, C.-F. Li, and G.-C. Guo, "Polarization nondegenerate fiber Fabry-Perot cavities with large tunable splittings," Appl. Phys. Lett. **112**, 171105 (2018).
47. J. Goldwin, S. Inouye, M. L. Olsen, B. Newman, B. D. DePaola, and D. S. Jin, "Measurement of the interaction strength in a Bose-Fermi mixture with ^{87}Rb and ^{40}K," Phys. Rev. A **70**, 021601 (2004).
48. M. Greiner, I. Bloch, T. W. Hänsch, and T. Esslinger, "Magnetic transport of trapped cold atoms over a large distance," Phys. Rev. A **63**, 031401 (2001).
49. S. Kuhr, W. Alt, D. Schrader, M. Müller, V. Gomer, and D. Meschede, "Deterministic delivery of a single atom," Science **293**, 278 (2001).
50. T. L. Gustavson, A. P. Chikkatur, A. E. Leanhardt, A. Görlitz, S. Gupta, D. E. Pritchard, and W. Ketterle, "Transport of Bose-Einstein condensates with optical tweezers," Phys. Rev. Lett. **88**, 020401 (2001).
51. J. Léonard, M. Lee, A. Morales, T. M. Karg, T. Esslinger, and T. Donner, "Optical transport and manipulation of an ultracold atomic cloud using focus-tunable lenses," New J. Phys. **16**, 093028 (2014).
52. F. Ferri, A. La Rooij, C. Lebouteiller, P.-A. Bourdel, M. Baghdad, S. Schwartz, S. Garcia, J. Reichel, and R. Long, "An optical elevator for precise delivery of cold atoms using an acousto-optical deflector," New J. Phys. **24**, 043013 (2022).
53. T. Kampschulte and J. Hecker Denschlag, "Cavity-controlled formation of ultracold molecules," New J. Phys. **20**, 123015 (2018).
54. D. Wellnitz, S. Schütz, S. Whitlock, J. Schachenmayer, and G. Pupillo, "Collective dissipative molecule formation in a cavity," Phys. Rev. Lett. **125**, 193201 (2020).
55. J. Galego, F. J. Garcia-Vidal, and J. Feist, "Cavity-induced modifications of molecular structure in the strong-coupling regime," Phys. Rev. X **5**, 041022 (2015).
56. J. Flick, M. Ruggenthaler, H. Appel, and A. Rubio, "Atoms and molecules in cavities, from weak to strong coupling in quantum-electrodynamics (QED) chemistry," Proc. Natl. Acad. Sci. U.S.A. **114**, 3026 (2017).
57. Y. Pan, L. Li, X. Zhou, D. Huang, Z. Shen, J. Wang, C. Li, and G. Guo, "Feedback and compensation scheme to suppress the thermal effects from a dipole trap beam for the optical fiber microcavity," Opt. Express **30**, 46280 (2022).
58. Z.-M. Shen, X.-L. Zhou, D.-Y. Huang, Y.-H. Pan, L. Li, J. Wang, C.-F. Li, and G.-C. Guo, "Continuously and widely tunable frequency-stabilized laser based on an optical frequency comb," Rev. Sci. Instrum. **94**, 023001 (2023).
59. P. Maunz, T. Puppe, I. Schuster, N. Syassen, P. W. H. Pinkse, and G. Rempe, "Normal-mode spectroscopy of a single-bound-atom–cavity system," Phys. Rev. Lett. **94**, 033002 (2005).
60. A. Boca, R. Miller, K. M. Birnbaum, A. D. Boozer, J. McKeever, and H. J. Kimble, "Observation of the vacuum Rabi spectrum for one trapped atom," Phys. Rev. Lett. **93**, 233603 (2004).
61. J. Gallego, W. Alt, T. Macha, M. Martinez-Dorantes, D. Pandey, and D. Meschede, "Strong purcell effect on a neutral atom trapped in an open fiber cavity," Phys. Rev. Lett. **121**, 173603 (2018).
62. J. Dalibard and C. Cohen-Tannoudji, "Laser cooling below the Doppler limit by polarization gradients: simple theoretical models," J. Opt. Soc. Am. B **6**, 2023 (1989).
63. J. A. Devlin and M. R. Tarbutt, "Three-dimensional Doppler, polarization-gradient, and magneto-optical forces for atoms and molecules with dark states," New J. Phys. **18**, 123017 (2016).